THE JOURNAL OF PHYSICAL CHEMISTRY B

Article

Cite This: J. Phys. Chem. B XXXX, XXX, XXX−XXX

pubs.acs.org/JPCB

Melting Transition of Oriented DNA Fibers Submerged in Poly(ethylene glycol) Solutions Studied by Neutron Scattering and Calorimetry

Adrián González,[†,‡] Andrew Wildes,[*,†] Marta Marty-Roda,[‡] Santiago Cuesta-López,[‡] Estelle Mossou,[†,§] Andrew Studer,[∥] Bruno Demé,[†] Gaël Moiroux,[⊥,#] Jean-Luc Garden,[⊥,#] Nikos Theodorakopoulos,[▽,○] and Michel Peyrard[◆]

[†]Institut Laue Langevin, 71, avenue des Martyrs - CS20156 - 38042 Grenoble Cedex 9 - France

[‡]ICCRAM, University of Burgos, Plaza Misael Bañuelos, 09001 Burgos, Spain

[§]Faculty of Natural Sciences, Keele University, Staffordshire ST5 5BG, United Kingdom

[∥]ANSTO, Locked Bag 2001, Kirrawee DC, NSW 2232, Australia

[⊥]Institut Néel, University Grenoble Alpes, F-38042 Grenoble, France

[#]Institut Néel, CNRS, 25 Avenue des Martyrs, F-38042 Grenoble, France

[▽]Fachbereich Physik, Universität Konstanz, D-78457 Konstanz, Germany

[○]Theoretical and Physical Chemistry Institute, National Hellenic Research Foundation, Vasileos Constantinou 48, 116 35 Athens, Greece

[◆]Université de Lyon, Ecole Normale Supérieure de Lyon, Laboratoire de Physique, CNRS, UMR 5672, 46 allée d'Italie, F-69364 Lyon Cedex 7, France

ABSTRACT: The influence of molecular confinement on the melting transition of oriented Na-DNA fibers submerged in poly(ethylene glycol) (PEG) solutions has been studied. The PEG solution exerts an osmotic pressure on the fibers which, in turn, is related to the DNA intermolecular distance. Calorimetry measurements show that the melting temperature increases and the width of the transition decreases with decreasing intermolecular distance. Neutron scattering was used to monitor the integrated intensity and width of a Bragg peak from the B-form of DNA as a function of temperature. The data were quantitatively analyzed using the Peyrard−Bishop−Dauxois model. The experiments and analysis showed that long segments of double-stranded DNA persist until the last stages of melting and that there appears to be a substantial increase of the DNA dynamics as the melting temperature of the DNA is approached.

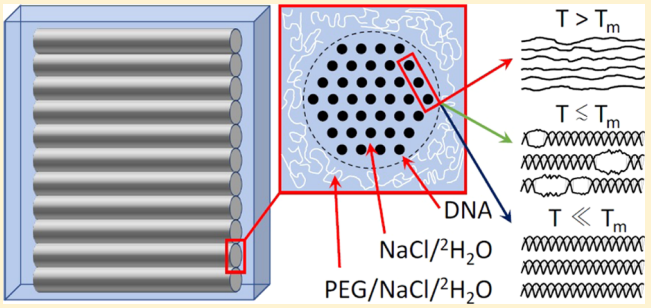

INTRODUCTION

The melting transition of DNA is the process in which an increase in temperature causes the hydrogen bonds between the base pairs to break. As the temperature rises, an increasing number of base pairs separate until the two strands of the double helix completely denature.

The thermal denaturation of this life-essential molecule has been extensively studied to learn the intramolecular interactions, the impact of the base pair sequence on DNA unwinding, and the effect of the solvent on DNA stability.[1−3] A better understanding of the transition could have an immediate impact on applications such as high-resolution melting analysis[4] or polymerase chain reactions,[5] which are widely used in biolabs around the world. However, the melting of DNA is itself interesting to study from a theoretical point of view because it is essentially a phase transition in a one-dimensional system.

Experimentally, the transition has been studied with techniques that probe either the bulk, like calorimetry, UV−vis absorption, and circular dichroism, or localized points on the molecule, like fluorescence. These techniques cannot access the spatial structure of the DNA molecules and so they cannot determine how the open and closed base pairs are distributed during the transition. Knowledge of spatial correlations and how they evolve with temperature is necessary for a complete understanding of the transition.

Received: November 25, 2017
Revised: January 19, 2018
Published: February 7, 2018

DOI: 10.1021/acs.jpcb.7b11608
J. Phys. Chem. B XXXX, XXX, XXX−XXX

Scattering techniques are able to access structural information and thus give information on the spatial correlations within the molecule. Such information is more easily accessible when the sample has a long-range order, which gives rise to Bragg peaks. DNA fibers, in which the molecules are coaligned and under close packing, have sufficient long-range order to give Bragg peaks. The advantage of focusing the study on Bragg peaks is that the information of interest is collected in a measurement that is only weakly perturbed by sample imperfections and incoherent contributions to the scattering.

The melting transition of an oriented fiber DNA has been previously studied[6,7] using neutron scattering, and the results were modeled with the mesoscopic statistical−mechanical Peyrard−Bishop−Dauxois (PBD) model.[8] The PBD model calculates the melting behavior of a single, isolated DNA molecule. The model successfully reproduced the observed temperature-dependent behavior of neutron scattering, showing that some long segments of double-stranded DNA persisted until the very last stages of the melting transition. However, the model does not account for interactions between the DNA molecules, which will be present in the close-packed environment of a fiber. The restricted degrees of spatial freedom due to confinement could arguably have an impact on the interpretation of the data. This article reports a study to determine whether spatial confinement of DNA has an impact on the melting transition and on the ability of the PBD model to reproduce the transition.

The method chosen to test the influence of confinement was immersion of fibers in a solution. The previous studies[6,7] used fibers whose water content was controlled via a humid atmosphere. The fibers swell if immersed, changing the distance between the molecules and allowing the influence of spatial confinement to be probed. However, the fibers can potentially dissolve if immersed. The use of scattering techniques to measure Bragg peaks requires that the high degree of orientation imposed by the fiber structure must be preserved. The solution must be carefully chosen to allow the fiber to swell without losing its orientation and, in the worst case, dissolving it.

A saline solution containing a high-molecular-weight (MW) polymer, such as poly(ethylene glycol) (PEG), is an ideal candidate. If PEG does not penetrate the DNA fibers, the osmotic pressure applied by the PEG acts analogously to a mechanical and permeable piston, preventing DNA from dissolving, thus preserving the long-range order, while allowing water and salt to be exchanged between the fibers and the solution. This osmotic pressure method has been reported in numerous articles.[9,10] X ray diffraction has proved that fibers equilibrated with these kind of solutions show a well-defined interaxial distance between molecules, which increases with decreasing concentration of the added polymer.[10]

A pilot experiment on fibers submerged in a PEG solution has been successfully performed and reported previously.[11] It proved that it is possible to follow the DNA melting transition using scattering techniques on a submerged sample, but the quality of the data was insufficient for a quantitative modeling by theory. The pilot experiment was performed with 20 000 MW PEG, and it was concluded that the experiment could be improved using a much lower molecular weight PEG. The molecular weight must not be so low, however, that the PEG can penetrate the fiber and influence the melting transition.

In this article, the results of a study of Na-DNA fiber samples submerged in four different PEG solutions using neutron scattering are presented and quantitatively analyzed in terms of the PBD model. The results of an extensive calorimetry investigation on similar samples are also reported, which provide a thermodynamical view of the bulk transition.

METHODS

Sample Preparation. Oriented Na-DNA fibers were made from natural salmon DNA purchased from Sigma-Aldrich (Salmon testes Fluka). The fibers were prepared from a solution of Na-DNA with sodium counter ions (1.58 g/L^{-1} Na-DNA and 0.15 M NaCl). The wet spinning method[12] was used to create samples of sufficient size and quality for a neutron scattering experiment. Details of the preparation have been reported in previous publications.[13,14] After spinning, the fibers were initially stored under a 75% humidified atmosphere created by a supersaturated NaCl solution for several weeks. Afterward, the fibers were humidified to 92% in a ^2H_2O atmosphere using a supersaturated potassium nitrate (KNO_3) solution. With this humidity, the DNA molecules adopt the B-conformation.[14] Some samples were kept under these conditions as a control, and these samples will be subsequently referred to as humidified fibers.

Solutions of 6000 and 8000 MW PEGs (hereafter referred to as PEG6k and PEG8k, respectively) were made for submerging the fibers. These molecular weights have been shown to be close to the lightest weight that can be used in the osmotic pressure method, with lower-MW PEGs known to penetrate into the DNA fibers.[15] PEG was dissolved in a buffer made with ^2H_2O with 0.1 M NaCl, 10 mM Tris, and 1 mM ethylenediaminetetraacetic acid at pD 7. ^2H_2O was used as ^2H has a much lower incoherent cross section for neutrons than that of ^1H; hence, the signal-to-noise ratio for the Bragg peaks would be much larger. The concentration range was $5 < C_{\%} < 40$, where $C_{\%} = 100 \times$ weight of polymer/total weight of the solution, which corresponds to osmotic pressures that have been shown to allow a substantial variation in the intermolecular DNA spacing while preventing the DNA from dissolving.[9,10,15] The solutions were degassed by subjecting them to a vacuum for 30 min.

Calorimetry. Four different kinds of samples were studied with differential scanning calorimetry (DSC): fiber samples submerged in PEG6k and PEG8k solutions, fibers submerged in the buffer used for preparing the PEG solutions, humidified fibers at 92% relative humidity (RH), and a dilute solution of the same DNA used to prepare the fibers dissolved in the buffer. For preparing the set of submerged samples, fibers with mass approximately 25 mg when dry were submerged in 0.5 mL of the appropriate solution. Note that submersion in a PEG-free buffer caused partial dissolution of the fibers, but due to the relatively low solubility of DNA in water (10 mg/mL for a saline buffer according to the provider), most of the DNA remained in a fiber form. The DNA concentration of the dissolved sample was 2 mg/mL, and the volume of solution measured was 0.33 mL.

The instrument used for measuring the fiber DNA samples was Micro DSC III (Setaram), whereas Nano DSC III (Calorimetry Science Corp.) was used to measure the dissolved DNA sample. The heating and cooling rate, β, was set to 1 °C/min in every case. On both instruments, the differential heat flux, ΔP, was measured between the sample and a reference tube. The DNA solution and the fibers submerged in buffer were measured with respect to the Na-^2H_2O buffer, whereas the

DOI: 10.1021/acs.jpcb.7b11608
J. Phys. Chem. B XXXX, XXX, XXX−XXX

PEG samples were measured with respect to their corresponding PEG solutions. The humidified fibers were measured with respect to an empty reference tube.

Prior to measuring the submerged fibers and dilute DNA solutions, calorimetric curves were recorded with the reference solution in both the sample and reference tubes. These curves were subtracted from the ΔP measured for the DNA-containing samples to account for instrumental artifacts. For the humidified fibers, a measurement was made with both sample and reference tubes empty, and this signal was subtracted from the sample data.

The differential heat capacity, ΔC, was calculated using ΔP with the following equation

$$\Delta C = -\frac{\Delta P}{\beta} - \tau\frac{\mathrm{d}(\Delta P)}{\mathrm{d}T} \quad (1)$$

where T is the temperature and τ is an instrument response constant, which was approximately equal to 60 s for both calorimeters. The specific heat of DNA was then given by $\Delta c = \Delta C/m_{\mathrm{DNA}}$, where m_{DNA} is the mass of DNA. A pretransition to post-transition baseline was subtracted; thus, the melting profile is relative to 0. Because Δc before and after the transition is roughly constant, the specific selection of this baseline does not affect the calculation of the parameters of the transition. The fraction of closed base pairs as a function of temperature ($f_{\mathrm{DS}}(T)$) was calculated using $\Delta c(T)$

$$f_{\mathrm{DS}}(T) = 1 - \frac{\int_{T_{\min}}^{T} \Delta c(T)\,\mathrm{d}T}{\int_{T_{\min}}^{T_{\max}} \Delta c(T)\,\mathrm{d}T} \quad (2)$$

where $T_{\min}$ and $T_{\max}$ are the minimum and maximum temperatures of the calorimetric scan. The melting temperature of the transition, T_{m}, is then defined as the temperature for which $f_{\mathrm{DS}} = 0.5$. The transition peak was fitted with a Gaussian function, and the width of the transition was identified with the full width half-maximum of the fit. Values of T_{m} and width presented in this article are the average of up to three measurements on identical samples, and the error bars ascribed to the data are the standard deviations of the measurements.

Neutron Scattering. Each sample for neutron scattering consisted of around 0.6 g of DNA fibers, which were concertina-folded and placed with their axes coaligned in a square aluminum cassette. The volume of the samples in the cassettes was roughly 20 × 20 × 2 mm^3. The cassettes were sealed using a lead wire. The humidified fibers were sealed in their 92% RH atmosphere, and the rest of the samples were submerged in roughly equal volumes of the appropriate solution of PEG before sealing. The samples were left to equilibrate with the liquid for a week before being measured. Four samples of DNA submerged in PEG solutions were studied by neutron scattering: the solutions containing PEG6k-17%, PEG6k-20%, PEG8k-15%, and PEG8k-20%. These concentrations were chosen because clear and intense Bragg peaks could not be obtained with samples containing lower or higher PEG concentrations. With lower concentrations, the relatively low osmotic pressures did not maintain enough long-range order. With higher concentrations, the contribution of PEG to the scattering engulfed most of the DNA signal.

The scattering geometry was depicted in previous publications.[11] The incident neutrons had wave vector $\vec{k}_{\mathrm{i}}$ and were scattered with an angle 2θ to a final direction $\vec{k}_{\mathrm{f}}$. The scattering vector, or momentum transfer, was $\vec{Q} = \vec{k}_{\mathrm{i}} - \vec{k}_{\mathrm{f}}$. Thus, its magnitude was as follows: $Q = 4\pi \sin(\theta)/\Lambda$, where Λ is the wavelength of the incident neutrons.

For each data set, the detector position was fixed and data were measured as a function of the sample rotation around the axis normal to the scattering plane; thus, selected parts of the reciprocal space were explored. The data were corrected for sample self-attenuation.

The scattering data were plotted using a convention, previously reported,[14] in which orthogonal reciprocal space directions are defined: $\vec{Q} = \vec{Q}_{\parallel} + \vec{Q}_{\perp x} + \vec{Q}_{\perp y}$. $\vec{Q}_{\parallel}$ is parallel to the fiber axis, $\vec{Q}_{\perp x}$ is normal to the plane of the cassette, and $\vec{Q}_{\perp y}$ is perpendicular to the fiber axis and is in the plane of the cassette.

The samples were measured using the D19 and D16 diffractometers at the Institut Laue-Langevin (France) and the WOMBAT powder diffractometer at the OPAL research reactor (Australia).

D16 was configured with a graphite monochromator. The incident wavelength was 4.55 Å. The monochromator−sample distance was 2.9 m. Presample collimation and beam size were defined with two slits: one rectangular (120 × 25 mm^2 $H \times W$) at 100 mm from the monochromator and another squared (25 × 25 mm^2) at 50 mm from the sample. A beryllium filter was used to suppress high-order contamination, and data were collected with its 320 × 320 mm^2 detector at several 2θ angles. There was no collimation between the sample and the detector.

D19 was also configured with a graphite monochromator delivering an incident wavelength of 2.4 Å. The monochromator−sample distance was 3.18 m. Presample collimation and beam size were defined with two sets of squared slits (12 × 12 mm^2) and a circular aperture (diameter of 10 mm). The slits were at 1.51 and 2.49 m from the monochromator. The circular aperture was at 3.1 m from the monochromator. High-order Bragg contamination was eliminated using a graphite filter. D19 has a 120° position-sensitive detector, which was fixed throughout the experiment. There was no collimation between the sample and the detector.

WOMBAT was used with a germanium monochromator. The monochromator−sample distance was 2.5 m. Presample collimation and beam size were defined with a set of rectangular slits (17 × 25 mm^2 $H \times W$) at 160 mm from the sample. The position-sensitive detector was fixed for the measurements. A beryllium filter was again used to suppress high-order contamination. An oscillating radial collimator of 0.5° between sample and detector positions was used for background suppression.

Two sets of measurements were made:

1. D16 and WOMBAT (with a wavelength of 5.66 Å) were used to record wide reciprocal space maps at room temperature to characterize the samples. The maps were measured with the fiber axis within and normal to the scattering plane. The maps were consistent with what was previously observed for humidified[14] and PEG samples.[11] Of particular interest was the strong Bragg peak centered at $\vec{Q}_{\parallel} \approx 1.87$ Å^{-1} when the fiber axis was in-plane, corresponding to the average distance between consecutive base pairs of $a_{\mathrm{bp}} \approx 3.14$ Å. This is the Bragg peak previously studied in ref 16, and it proves that the samples were in a semicrystalline B-form.
2. D19 and WOMBAT (with a wavelength of 4.62 Å) were used to record the temperature-dependent evolution of the Bragg peak at $\vec{Q}_{\parallel} \approx 1.87$ Å^{-1}. Reciprocal space maps with the fiber axis within the scattering plane ($\vec{Q}_{\perp y} = 0$)

DOI: 10.1021/acs.jpcb.7b11608
J. Phys. Chem. B XXXX, XXX, XXX−XXX

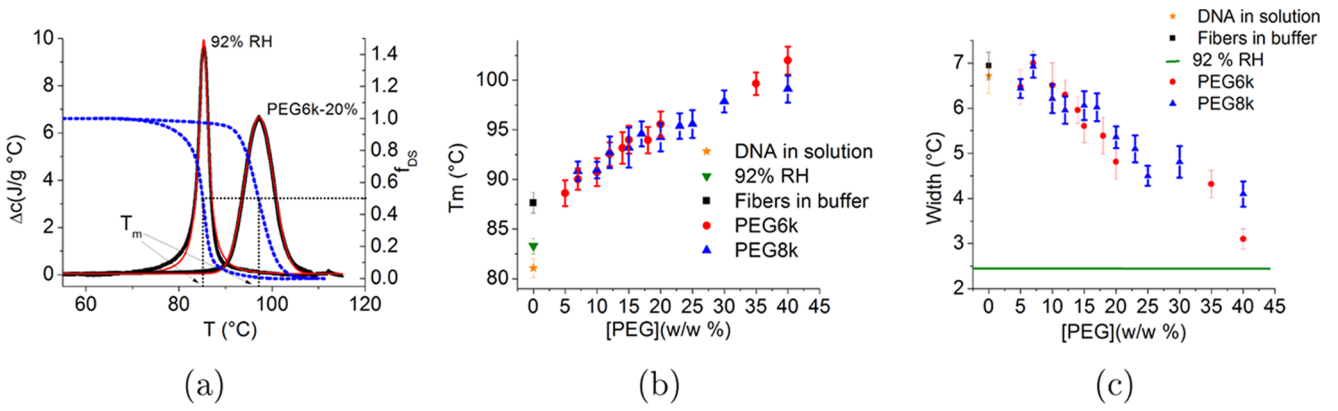

Figure 1. (a) Heat capacities per unit mass, Δc, for Na-DNA fibers equilibrated in a 92% humid atmosphere and submerged in a solution of PEG6k-20% w/w are plotted with solid thick black lines, the solid thin red lines represent the fit to the data, and the blue dashed lines represent the fraction of closed base pairs as a function of temperature. The T_m's are highlighted. (b) Melting temperature measured by DSC of the DNA dissolved in the buffer without PEG, DNA fibers humidified at 92% RH, fibers submerged in the buffer, and fibers submerged in solutions of PEG6k and PEG8k as a function of the PEG concentration. (c) Width of the transition as seen by DSC for the same samples as shown in panel (b) as a function of the PEG concentration. The green line marks the value of the width for the humidified fibers. The error bars represent the standard deviation of measurements on identical samples.

were collected at several temperatures between 20 and 110 °C. Then, data along $\vec{Q}_{\parallel}$, when $\vec{Q}_{\perp x} = 0$, were extracted for each temperature. These cuts through the maps go through the center of the Bragg peak.

Two different sample environments were used. On D19, two heating elements were attached to the opposite vertices of the square cassette. This gave a temperature stability of around ±0.2 °C at room temperature, but thermal oscillations increased with temperature. The temperature stability was roughly ±1 °C at 95 °C, corresponding to the T_m of the PEG6k-17% sample. On WOMBAT, a flow of heated air was used. On this instrument, a technical problem with maintaining the rate of the air flow affected the thermal stability at high temperatures when measuring the PEG6k-20% sample. The problem was corrected for subsequent measurements. The thermal stability was around ±1 °C at 95 °C for the PEG6k-20% sample and <0.1 °C over the whole temperature range for the PEG8k-15% and PEG8k-20% samples.

The raw experimental neutron data from D16 and D19 are separately accessible.[17]

RESULTS

Differential Scanning Calorimetry. The calorimetry data for every sample showed a well-defined peak, related to the excess heat capacity of the melting transition. Figure 1a shows the specific heat as a function of temperature for a humidified fiber and a sample submerged in a solution of PEG6k-20%, along with the respective fits to the curves. The fraction of closed base pairs for each sample, calculated using eq 2, is also plotted. The melting temperatures corresponding to the temperature at which half of the base pairs are open are highlighted.

Figure 1b shows melting temperatures for the samples. The T_m's for the immersed fibers were all higher than those for the dilute DNA solution. T_m increases linearly with increasing PEG concentration, and the increase does not appear to depend on the molecular weight of PEG.

Figure 1c shows the widths of the melting transition for the samples. The width is the same for the dilute DNA solution and for fiber DNA immersed in buffer without PEG. The widths decrease linearly with increasing PEG concentration, and, as for the melting temperature, the behavior is the same for PEG6k and PEG8k.

The melting temperature and width for the humidified fibers are included for completeness in Figure 1b,c. The melting temperature is similar to that for the dilute DNA solution and is less than that for immersed fibers. The width is narrower than for any of the other samples. Comparisons between the humidified fiber and the other samples, however, must be made with caution as the former sample will have very different water and Na^+ contents. The melting transition is strongly affected by water and ion activities,[18] which are approximately equivalent for the immersed fibers[10] and the dilute DNA solution but will be different for the humidified fibers. Consequently, it is very difficult to attribute a definitive reason behind the calorimetric differences between the humidified sample and the others.

Packing Structure of the Molecules. Reciprocal space maps were recorded for two sample orientations, with the fiber axis within and normal to the scattering plane. The maps represent the diffracted intensity in reciprocal space using the perpendicular coordinate system introduced in the Methods section: ($\vec{Q}_{\parallel}$, $\vec{Q}_{\perp x}$, $\vec{Q}_{\perp y}$). They all are qualitatively identical to what was presented in previous studies for B-form DNA.[11,19] The features of the submerged samples were smaller in magnitude and broader in the sample rotation angle with respect to the humidified fibers as observed previously.[11] This suggests that some orientation of the fibers has been lost due to the submersion. However, the samples retained enough orientation to give strong Bragg peaks.

The reciprocal space maps collected with the fiber axis normal to the scattering plane ($\vec{Q}_{\parallel} = 0$) showed two strong ringlike features at low Q, as observed previously.[11] These reflections are at constant Q, or, equivalently, at constant 2θ. These are Bragg peaks arising from correlations in the direction perpendicular to the molecular axis. They relate to the packing structure of the molecules in the fiber. These measurements were used to calculate the intermolecular distance of the different samples and thus to gauge the effect of the PEG solutions on the confinement of the molecules. The data of these maps were summed over the sample rotation angles and plotted as a function of the magnitude of the scattering vector. The results can be seen in Figure 2.

DOI: 10.1021/acs.jpcb.7b11608
J. Phys. Chem. B XXXX, XXX, XXX−XXX

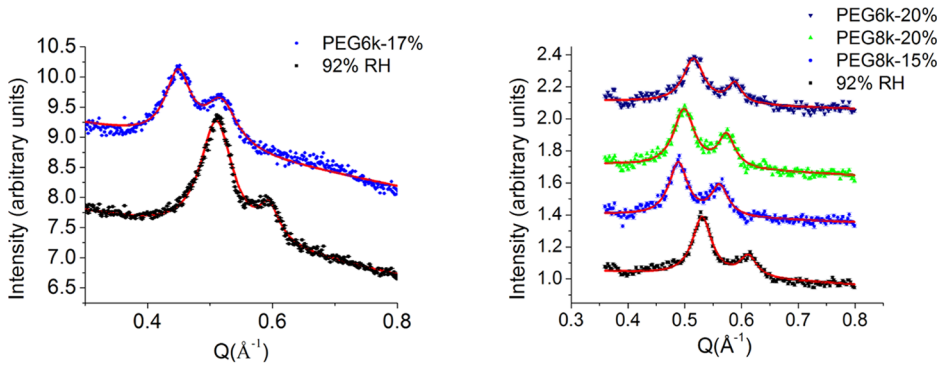

(a) Samples measured in D16 (b) Samples measured in WOMBAT.

Figure 2. Sum of the intensities over the sample rotation angles of data collected with the fiber axis normal to the scattering plane for a constant scattering vector as a function of Q. The curves have been shifted vertically for the sake of clarity. The red lines represent the fits to the data.

The peaks for the submerged samples are shifted to lower Q values with respect to those of the humidified fibers. This reflects an increase in the lattice parameters, which is consistent with the fiber swelling when submerged. B-form DNA fibers are believed to have a hexagonal space group, as shown for the B-form Na-DNA at 92% RH by Langridge and Wilson[20] and for samples submerged in PEG solution by Podgornik et al.[10] The two peaks can be indexed as the 110 and 200 reflections, respectively, from the hexagonal lattice. The d-spacing related to a given peak is $d = 2\pi/Q_C$, where Q_C is the center of the peak, and the relation between the Miller indices and lattice parameter a, corresponding to the axis-to-axis distance between two molecules, is $a = d\left(\frac{4}{3}(h^2 + kh + k^2)\right)^{1/2}$.

The centers of the peaks for a given sample were determined by fitting two Lorentzian functions with a linear background. The results of the fits can be seen in Figure 2. The lattice parameter of the humidified sample was calculated using the average a from both peaks and was found to be $a_{Hu} = 24.66 \pm 0.09$ Å, which is consistent with previous results.[20] The intermolecular distances for the other samples were calculated accordingly, and the percentage increase in the intermolecular distance with respect to the humidified fibers was computed. Table 1 shows the values of the percentage increase for each sample.

Table 1. Percentage Increase in the Intermolecular Spacing for Na-DNA Fibers Submerged in PEG Solutions With Respect to the Humidified Fibers

sample	a (Å)	$\frac{\Delta a}{a_{Hu}}$ (%)
PEG6k-17%	28.24 ± 0.05	14.54 ± 0.91
PEG8k-15%	26.92 ± 0.06	9.18 ± 0.99
PEG8k-20%	26.11 ± 0.04	5.9 ± 0.81
PEG6k-20%	25.48 ± 0.03	3.33 ± 0.70
humid fibers	24.66 ± 0.09	0

Temperature Dependence of Neutron Scattering. Temperature-dependent scattering for four samples (PEG6k-17%, PEG6k-20%, PEG8k-15%, and PEG8k-20%) was collected to follow the evolution of the Bragg peak at $Q_{\|} \approx 1.87$ Å^{-1}. The integrated intensity of the peak is directly proportional to the number of closed base pairs in the intact double-helical domains. As the temperature rises and the base pairs dissociate, the integrated intensity of the peak will fall. The width of the Bragg peak is inversely proportional to the average size of the intact double-helical domains. It gives access to the evolution of the correlation length of the molecule as a function of temperature.

Two cassettes containing PEG-only solutions were prepared. The cassettes contained PEG6k-17% and PEG6k-20% respectively. The temperature-dependent scattering of each was measured to account for the contribution of the PEG solution to the scattering of the sample. The changes in the scattering of the solutions with temperature were negligible.

The cuts along $\vec{Q}_{\|}$ at $\vec{Q}_{\perp x} = \vec{Q}_{\perp y} = 0$ in the maps of the DNA samples for every temperature were concatenated to create Figure 3. Each scan showed a mixture of Bragg and diffuse scattering. The Bragg scattering consisted of the DNA Bragg peak at $\vec{Q}_{\|} \approx 1.87$ Å^{-1} and other Bragg peaks related to the material of the sample cassette. The diffuse contribution gave rise to a nonzero Q-independent background plus a broad bump underneath the Bragg peaks. The DNA Bragg peaks are relatively unchanged until high temperatures are reached, where they disappear. Every sample was cooled back to room temperature after the measurement at the highest T and then measured again. The Bragg peak was not recovered in any sample, showing that the DNA had completely melted at high T and the orientation given by the fiber structure had been lost. This is in contrast to the pilot study where heating was stopped before the melting transition was completed and a Bragg peak was recovered when the sample was cooled back to room temperature.[11]

The PEG6k-17% sample was measured on D19 and is shown in Figure 3a. The figure shows that there is an increase in the diffuse background as the transition is approached, particularly for $T \geq 97$ °C. This effect must be related to the DNA because the scattering from the PEG solution alone did not change significantly with T.

Figure 3b–d shows data from samples measured on WOMBAT. An increase in the diffuse scattering with temperature is present in these samples as well, but it is weaker and barely noticeable in these figures. The narrow peak appearing at ≈2.2 Å^{-1} in the WOMBAT data was attributed to a Bragg peak from the lead seal of the cassette. It did not appear in the D19 data because of the smaller footprint of the beam. The width of the beam on WOMBAT (25 mm) illuminated the lead seal of the cassette but on D19 the circular beam of diameter 10 mm did not.

DOI: 10.1021/acs.jpcb.7b11608
J. Phys. Chem. B XXXX, XXX, XXX–XXX

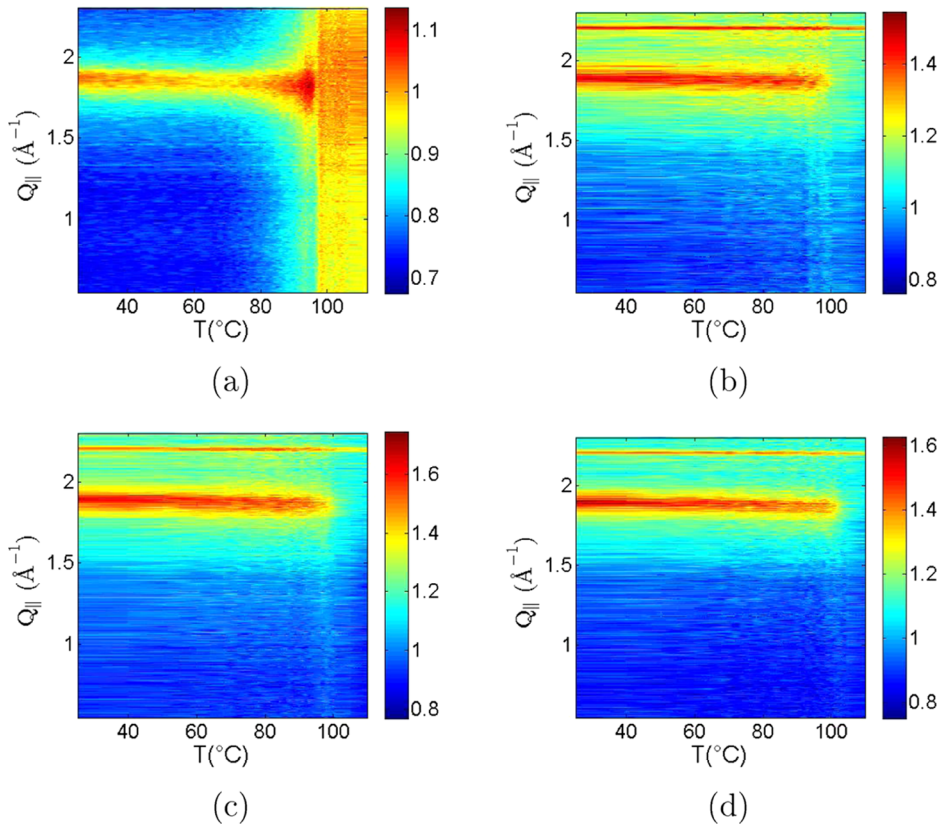

Figure 3. Temperature dependence of the $Q_{\|} \approx 1.87$ Å^{-1} Bragg peak for (a) the PEG6k-17% sample measured at D19 and the samples measured at WOMBAT: (b) PEG6k-20%, (c) PEG8k-15%, and (d) PEG8k-20%.

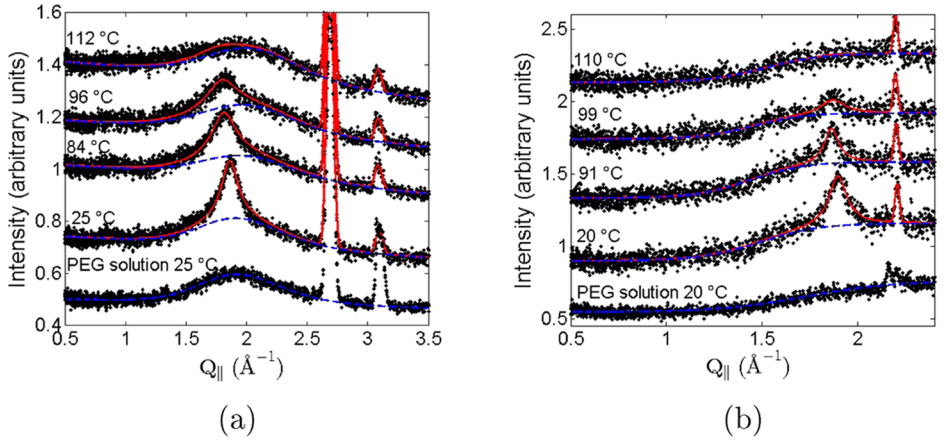

Figure 4. Representative examples of the temperature dependence of the $Q_{\|} \approx 1.87$ Å^{-1} Bragg peak and the PEG solution without DNA for (a) the PEG6k-17% sample measured at D19 and (b) the PEG6k-20% sample measured at WOMBAT. The red solid lines are the final fits to the data using eq 6, and the blue dashed lines are the fits to the diffuse scattering (eq 4). The curves have been shifted vertically for the sake of clarity.

Representative data for the $\vec{Q}_{\|}$ scans of the PEG6k-17% sample measured on D19 and for the PEG6k-20% sample measured on WOMBAT at different T's are shown in Figure 4a,b, respectively. The DNA Bragg peak at $\vec{Q}_{\|} \approx 1.87$ Å^{-1} is clearly visible. The figure includes a similar scan for the cassettes containing only the PEG solutions at room temperature. It shows that the diffraction from PEG generates a broad bump in the same $\vec{Q}_{\|}$ range as that for the DNA peak. The bump cannot be easily subtracted from the DNA curves due to the uncertainty in the liquid volumes of the two samples, meaning that the two data sets could not be accurately normalized on the same scale. The narrow peaks appearing at $\vec{Q}_{\|} \approx 2.6$ and 3.1 Å^{-1} in the D19 data are due to Bragg peaks from the aluminum of the cassette. The Q-range recorded on WOMBAT is smaller due to the longer wavelength used with respect to D19.

The DNA Bragg peak was fitted at every temperature to determine the integrated intensity and width. In previous studies performed on humidified fibers,[6] the peak could be fitted with a Lorentzian function on a constant background. Although a Lorentzian is still appropriate for the Bragg peak, the addition of the PEG solution to the DNA sample gave rise to added diffuse scattering that complicated the fitting of the peak. The origin of the diffuse scattering is not totally clear.

DOI: 10.1021/acs.jpcb.7b11608
J. Phys. Chem. B XXXX, XXX, XXX−XXX

The contribution of PEG is important, as shown in Figure 4, but DNA is also contributing because it is responsible for the part of the diffuse scattering that increases with temperature.

A Lorentzian function was used to describe the DNA Bragg peak, and the diffuse scattering was modeled using a phenomenological approach. The Bragg peak was modeled with

$$I_1(Q_{\|}) = \frac{I_0}{\pi}\frac{\gamma/2}{(Q_{\|} - Q_0)^2 + (\gamma/2)^2} \tag{3}$$

where I_0 is the integrated intensity of the peak, γ is the full width at half-maximum of the peak, and Q_0 is the peak center. The best results for fitting the diffuse scattering were achieved using a straight line plus a "double-step" function of the form

$$I_2(Q_{\|}) = A_0 + BQ_{\|} + \frac{A_1}{2}\left[\tanh\left(\frac{Q_{\|} - Q_1}{s_1}\right) - \tanh\left(\frac{Q_{\|} - Q_2}{s_2}\right)\right] \tag{4}$$

A_0 and B are, respectively, the intercept and slope of the straight line. The third and fourth terms in eq 4 generate a function with a rising step centered at Q_1 and a declining step centered at Q_2 with a plateau in between whose height is set by A_1. The gradients of the first and second steps are defined as s_1 and s_2, respectively. Finally, the Bragg peaks not related to DNA (Al and Pb) were accounted for with Gaussian functions

$$I_{\mathrm{Al,Pb}} = \sum_{\mathrm{i=Al,Pb}} \frac{A_i}{s_i\sqrt{2\pi}}\, e^{-(Q_{\|} - Q_{0,i})^2/2s_i^2} \tag{5}$$

where A_i are the integrated intensities of the Gaussian functions, $Q_{0,i}$ are their centers, and s_i are their variances.

The total intensity for every temperature was fitted with the following expression

$$I(Q_{\|}) = I_1 + I_2 + I_{\mathrm{Al,Pb}} \tag{6}$$

A_0 and B were not fit-parameters. Their values were calculated before fitting a given curve. For the D19 data, the average values of the scattering signal for $Q_{\|} < 0.6$ Å^{-1} and $Q_{\|} > 3.4$ Å^{-1} were calculated and a line was drawn between the two values. A_0 and B were taken as, respectively, the intercept and slope of that line. For the WOMBAT data, B was set to 0 and A_0 was determined by averaging the signal for $Q_{\|} < 0.8$ Å^{-1}. In addition, for the WOMBAT data, the diffuse scattering was represented by a single rising step function, so the term $\tanh\left(\frac{Q_{\|} - Q_2}{s_2}\right)$ in eq 4 related to the declining step was discarded.

The curves of the PEG solutions at room temperature were fitted using eq 4. The results can be seen in Figure 4a,b. The values for the parameters of this fit (A_1, Q_1, s_1, Q_2, s_2) were used as part of the initial set of values for fitting the DNA data at room temperature using eq 6. The rest of initial values were chosen by visual comparison. The final fitted parameters were robust.

For subsequent temperatures, a two-stage process was used to get an accurate fit when the size of the Bragg peak and the diffuse contribution became comparable. For a given temperature above room temperature T, the γ from the fit of the previous temperature was used to define a range in Q centered at around the DNA Bragg peak ($Q_0 - 0.8\gamma \le Q \le Q_0 + 0.8\gamma$). In the first stage, the parameters of the DNA Bragg peak (eq 3) were fixed, data inside the previously defined range were ignored, and eq 6 was fitted using the results for the fit of the previous temperature as initial values for the parameters. In the second stage, data outside the range were ignored, the parameters of eqs 4 and 5 were fixed to the fitted values of the first stage, and the DNA Bragg peak was fitted with eq 6. The two-stage process was repeated three times per temperature. Each new iteration used the parameters of the previous iteration as initial parameters for the fit. After three iterations, the parameters were stable.

The fitted values for eq 5 did not change within reasonable limits with T, which is consistent with the fact that no significant changes were expected from Al or Pb in the range of temperatures studied.

Examples of the fits can be seen in Figure 4. The fitting is very consistent but should be interpreted with care at high temperatures, where the Lorentzian peak was so small in comparison to that of the diffuse contribution that the general fit had trouble converging. At these temperatures, the values for γ and Q_0 were fixed to the values of the last temperature at which the fit converged and only I_0 was fitted.

Figure 5 shows the evolution of the A_0 parameter with temperature for all of the samples. $A_0(T)$ in this figure is normalized by its value at T = 20 °C to allow easy comparison between samples. $A_0(T)$ describes adequately the magnitude of the increase of diffuse scattering with T. The figure proves that the diffuse contribution rises close to the melting temperature in every sample. The increase at the highest T reached is approximately 20% in D19 data and approximately 5% in WOMBAT data. It is likely that this quantitative difference, clearly visible on comparing Figure 3a with Figure 3b−3d, is due to the different instrument configurations. There are two factors that likely to contribute to the difference.

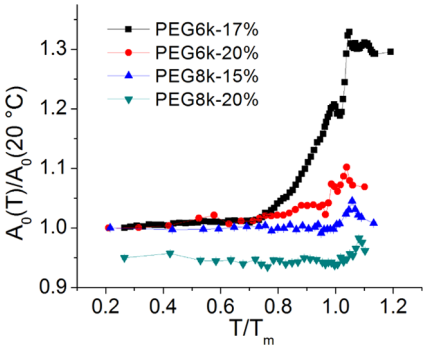

Figure 5. Parameter A_0 from eq 4 as a function of the reduced temperature (T/T_m calculated in celsius) normalized by its value at 20 °C for each sample. A_0 is the average of the intensity at low Q and represents the magnitude of the diffuse contribution. The results come from the quantitative analysis of the data in Figure 3. The curve related to the PEG8k-20% sample is shifted downward by 0.05 units for the sake of clarity.

The first concerns the collimation between the sample and the detector. D19 had no collimation, whereas WOMBAT used an oscillating collimator. In principle, an oscillating collimator limits only the scattering gauge volume of the sample. However, the diffuse scattering resembles, to first order, incoherent scattering, whereas the scattering angles for the Bragg peaks are reasonably well self-collimated. The WOMBAT oscillating

DOI: 10.1021/acs.jpcb.7b11608
J. Phys. Chem. B XXXX, XXX, XXX−XXX

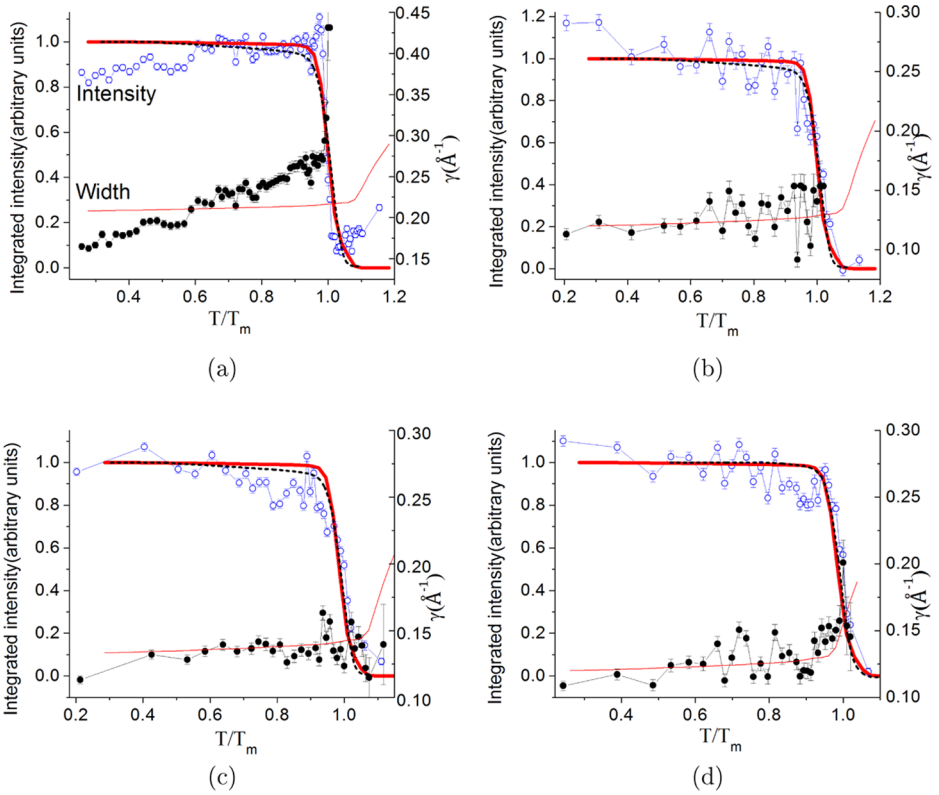

Figure 6. Comparison between theory and experiment for the Bragg peak and calorimetry data of the sample submerged in (a) PEG6k-17% measured on D19 and the samples submerged in (b) PEG6k-20%, (c) PEG8k-15%, and (d) PEG8k-20% and measured on WOMBAT . The Bragg peak results come from the quantitative analysis of the data in Figure 3. Reduced temperature T/T_m (calculated in celsius) was used, where T_m is the melting temperature of the sample. In each panel, the three upper curves relate to the scale in the left. They are the fitted integrated intensity to the Bragg peaks I_0 (blue open circles), the theoretical integrated intensity (thick red line), and the fraction of closed base pairs calculated with calorimetry for a corresponding sample (black dashed line); the fitted integrated intensities have been divided by arbitrary numbers for easy comparison. The lower curves relate to the scale in the right. They are γ, the fitted widths of the Bragg peaks (black closed circles), and the theoretical widths of the peaks (thin red lines).

collimator also limits instantaneously the divergence of the scattered beam to 0.5°, thus reducing an incoherent contribution relative to a coherent signal. This partly explains the larger diffuse signal in the D19 data.

The second concerns the kinematic limits on the energy integration of the neutron instrument. Neither WOMBAT nor D19 had any means to analyze the final energy of the neutron. Both instruments therefore integrated over neutron energy transfers. The allowed energy and momentum transfers are limited by the energy of the incident neutrons, which was 14.20 meV for D19 and 3.83 meV for WOMBAT. D19 therefore integrated over a much larger energy window than WOMBAT. Fiber DNA has substantial spectral weight from 2 to 25 meV,[21] and D19 captured these lattice dynamics where WOMBAT could not. The dynamics of DNA will change substantially as the melting temperature is approached, giving a nonlinear increase in the spectral weight for all Q and proportionately more diffuse scattering in the D19 data.

Figure 5 also shows that the values for A_0 do not increase monotonically with temperature close to melting, particularly for the PEG6k-17% (black squares) and the PEG6k-20% (red circles) samples. The data shows small peaks in A_0, which may also be observed in Figure 3a,b as vertical lines close to the temperature at which the Bragg peak disappears. As previously stated, the temperature stability at the melting temperatures for these samples was rather poor because of technical issues with the sample environments. The amplitude of the diffuse scattering increases rapidly with temperature in this range. The preliminary study[11] showed that the melting transition is, to some degree, reversible in these samples so long as the melting is not complete. It is probable that the variations in A_0 are coupled with the temperature stability and that the final registered values are indicative of the weighted average of the fluctuating intensity over the duration of the measurement.

Figure 6 shows the fitted I_0 and γ as a function of temperature for the four samples. For all samples, the intensities plummet and the peaks effectively disappear over the range $0.95 \leq T/T_m \leq 1.05$. For the WOMBAT data, the integrated intensities and widths stay roughly unchanged until close to the melting temperature, as seen in previous studies on humidified fibers.[6,7] This suggests that, as for humidified fibers, long segments of DNA remain until the very last stages of melting. These define the width of the Bragg peak. At the temperature where these last segments denature, the intensity of the Bragg peak is so weak that it is lost in the diffuse scattering and any change in the width cannot be unambiguously determined from a fit.

The PEG6k-17% sample measured on D19 shows a somewhat different behavior. Both I_0 and γ increase steadily before the T_m. This difference in the behavior of the fitted parameters with respect to the WOMBAT data may be related to the different integration over neutron energy transfers for both instruments. An increase in the phonon dynamics with increasing temperature can manifest itself as an increasing

DOI: 10.1021/acs.jpcb.7b11608
J. Phys. Chem. B XXXX, XXX, XXX−XXX

width in the tails of a Bragg peak. Such an effect would be more dramatic in D19 because of the expanded energy integration. Although a neutron inelastic scattering measurement would be necessary to prove the hypothesis, it appears likely that the increasing I_0 and γ with temperature seen on D19 are due to the increased dynamics of the fiber DNA as melting is approached.

Analysis. The PBD model was used to make a quantitative analysis of the fit results, following a previously reported procedure.[6,16] The model can be used to calculated the probability that a base pair of a given sequence is closed at a given temperature. The size and distribution of closed segments can then be determined. The expected diffraction pattern, $S(Q)$, from the sequence can then be calculated and compared to that from the experiments.

In the PBD model, the configuration energy of a DNA molecule of N base pairs is given by

$$H_y = \sum_{j=1}^{N-1} W(y_j, y_{j+1}) + \sum_{j=1}^{N} V_j(y_j) \tag{7}$$

where y_j represents the stretching of the jth base pair caused by the transverse displacement of the bases and $W(y_j, y_{j+1})$ is a potential describing the stacking interaction between adjacent bases[22]

$$W(y_j, y_{j+1}) = \frac{1}{2}k[1 + \rho\, e^{-b(y_j + y_{j+1})}](y_j - y_{j+1})^2 \tag{8}$$

where k is the coupling constant, ρ is the relative strength of the nonlinear base stacking, and b is the inverse range of the nonlinear base stacking. V_j describes the intrapair potential in the jth base pair and takes into account the hydrogen bonding, electrostatic interactions between phosphate groups, and solvent effects. It was assumed to be a Morse potential

$$V_j(y_j) = D_j[1 - e^{-\alpha_j y_j}] \tag{9}$$

D_j and α_j, respectively, being the depth and inverse range of the potential. Four different parameters were necessary for describing the two kinds of base pairs: D_{AT} and α_{AT} and D_{GC} and α_{GC}.

The relevant parameters for eq 7 were refined by comparing the calculated melting curve with the data from calorimetry. To determine the melting curve of a DNA molecule, it is necessary to differentiate between closed and open base pairs quantitatively. A base pair was considered to be closed if $y_j <$ 1.5 Å, consistent with previous calculations.[6]

A segment of the genome of Atlantic Salmon reported previously[23] (10 000 bases starting at site 50 000) was chosen for the calculation. In the modeling, W was assumed to be the same for all combinations of adjacent base pairs, which has been shown to be reasonable for describing the melting curves of long DNA molecules.[6,24] The DNA sequence was taken into account only for the calculation of the intrapair potential, V_j.

All values of the parameters of the Hamiltonian used to model the data, except for D_{AT} and D_{GC}, are the same as those previously used in the study of humidified fibers.[6] They are shown in Table 2. D_{AT} and D_{GC} represent the energy barrier for base pair dissociation and thus they are the main factors in setting the T_m of the theoretical melting curve. As shown in Figure 1b, the melting temperature when the fibers are submerged in the PEG solutions increases with PEG concentration. Thus, D_{AT} and D_{GC} needed to be scaled to reproduce the melting temperature of each sample. The values

Table 2. Parameters Used in the PBD Model

parameters	value
k	4.5×10^{-4} eV/Å^2
ρ	50
b	0.2 Å^{-1}
α_{AT}	4.2 Å^{-1}
α_{GC}	6.9 Å^{-1}
$D_{AT,95}$	0.13150 eV
$D_{GC,95}$	0.17150 eV

for the depth of the Morse potential shown in Table 2 ($D_{AT,95}$, $D_{GC,95}$) with the chosen sequence and parameters correspond to T_m = 95 °C. For a sample with a $T_m = T_{m,x}$ in celsius, the value for D_{AT} was scaled as

$$D_{AT,x} = D_{AT,95}\left(\frac{T_{m,x} + 273}{95 + 273}\right) \tag{10}$$

and an analogous expression was used for the value of D_{GC}.

The calculated $S(Q)$ for each T was fitted with eq 3 to determine the values of I_0 and γ as a function of T that could be compared with the experimental data.

The calculation of $S(Q)$ included an exponential term analogous to a Debye–Waller factor, which accounted for the structural and thermal disorders. The exponent of this term is proportional to Δ, which was calculated with expression $2\Delta = Q_\parallel^2(\langle\sigma^2\rangle + \langle\lambda^2\rangle)$.

$\langle\sigma^2\rangle$ is proportional to the longitudinal thermal motions of the DNA molecule and, as done previously,[6] was estimated using $\langle\sigma^2\rangle = k_B T/\mu c_0^2 a_{bp}^2$, where k_B is the Boltzmann constant, μ = 618 amu is the DNA mass per base pair, and c_0 = 2830 ms^{-1} is the sound velocity in DNA reported previously.[25]

$\langle\lambda^2\rangle$ is the standard deviation of the distance between consecutive base pairs and accounts for the structural disorder along the molecular axis. The value of $\langle\lambda^2\rangle$ = 0.18 Å, reported by Lavery et al.,[26] was used to model the melting of humidified DNA.[6] This gave widths for the Bragg peak that were too small in comparison to those of the submerged samples. $\langle\lambda^2\rangle$ was increased to model the current data. The values used can be found in Table 3.

Table 3. Standard Deviation of the Distance Between Consecutive Base Pairs Used to Calculated the $S(Q)$ of Each Sample

sample	$\langle\lambda^2\rangle$ (Å)
PEG6k-17%	0.45
PEG8k-15%	0.35
PEG8k-20%	0.33
PEG6k-20%	0.33
humid fibers	0.18

It is unlikely that the effects of PEG can directly modify the standard deviation of the distance between base pairs along the molecule. More likely, the increase of $\langle\lambda^2\rangle$ accounted phenomenologically for other disorder effects, such as an increased variation of the alignment of the molecules, when the fibers were submerged.

The Debye–Waller factor, 2Δ, is a function of both $\langle\sigma^2\rangle$ and $\langle\lambda^2\rangle$, and it is possible that the increased Bragg widths are at least partly due to thermal fluctuations that were not linear with temperature. However, without inelastic scattering data, it is not possible to say whether the larger widths were mainly due

DOI: 10.1021/acs.jpcb.7b11608
J. Phys. Chem. B XXXX, XXX, XXX–XXX

to the increased structural disorder, increased thermal fluctuations, or a combination of both factors.

Figure 6 shows a comparison of the experimental and theoretical integrated intensities and widths of the peaks for each sample along with the fractions of open base pairs calculated by calorimetry. The data are plotted as a function of reduced temperature, T/T_m, as there are differences between the absolute melting temperatures recorded with neutrons and calorimetry due to different sample environments.

Overall, the model matches all of the data quantitatively. The agreement is excellent for the samples measured on WOMBAT. Although the magnitudes for the model match the D19 data and the model does predict a linear increase in width with temperature, the model fails to adequately describe the gradient of the increasing width and of the integrated intensity with temperature below T_m. This may be an aspect of the modeling that does not fully capture the DNA phonon dynamics which, combined with the expanded energy integration on D19, is the possible cause of the increases in I_0 and γ. However, the magnitudes of the intensities and widths are matched and modeling may be regarded as satisfactory.

DISCUSSION

Calorimetry. Figure 1b shows that fibers submerged in buffer (no PEG, black square) have a higher melting temperature than that of DNA dissolved in the same buffer (orange star). Dissolved DNA is less confined than the DNA in the submerged fibers, and this is the only difference between these two samples. Thus, confinement must be the origin of the higher T_m for the fibers submerged in buffer without PEG. A similar effect has been previously reported[27] where the transition between DNA dispersed in the solution and aggregated in a liquid-crystalline state increased the T_m recorded by calorimetry. The observations are consistent with the hypothesis of Cherstvy and Kornyshev that an increase in molecular interactions as the space between molecules decreases can, in turn, lower the base pair free energy in the helical state and thus increase the melting temperature.[28]

The calorimetry data in Figure 1b show that the melting temperature of DNA fibers immersed in PEG solutions increases with the PEG concentration. Similar results have been reported for DNA dissolved in PEG solutions, and they were attributed to the excluded volume effect.[18,29] This assumes that the volume of the solution unavailable to the DNA due to the presence of PEG stabilizes the molecular conformation, which occupies the smallest space, that is, the helix molecule. However, PEG is not expected to penetrate the fibers in the range of concentrations and molecular weight used in the present study.[10] If PEG is on the outside of the fibers, it is in contact only with the DNA molecules on the surface of the fibers, which are a small percentage of the total number of DNA molecules in the sample. Thus, the excluded volume and specific interactions of the PEG are expected to have little-to-no effect on the recorded characteristics of the transition. Indeed, PEG6k and PEG8k seem to have the same trend, suggesting, following previous studies,[18] that the excluded volume is not affecting dramatically the T_m and verifying that PEG has not penetrated the fibers.

The interaxial distance in the fibers changes in the presence of PEG, as shown in Table 1 and observed previously.[9] Thus, changes in the confinement due to the presence of PEG seem to be a main factor in the observed relation between T_m and PEG concentration.

The calorimetry results published in the pilot study[11] suggest a similar trend. The measurements were performed on a fiber sample immersed in a 0.5 M NaCl solution with 10% (w/w) 20 000 MW PEG, which has a higher salinity and much higher PEG weight than those for the samples measured in Figure 1; however, they showed an increased melting temperature and width relative to those of a humidified fiber. The intermolecular distance was not measured for this sample, but measurements for a similar sample with 17% (w/w) 20 000 MW PEG showed the intermolecular spacing to be ≈2% larger than that for the humidified fiber, which is smaller than the values in Table 1. It is reasonable to suggest that 10% PEG would have a larger intermolecular spacing, comparable to the 3.33% increase found for the PEG6k-20% sample. The melting temperature in the pilot study was ≈95 °C, which is comparable to that found for PEG6k-20%. The data are therefore consistent with the hypothesis that confinement is a decisive factor in the eventual melting temperature.

Figure 1c shows how the width of the transition of submerged fibers decreases as the PEG concentration increases. The width of the transition is related with its cooperativity, i.e., the tendency of the base pairs to open in contiguous segments. Narrower transitions are more cooperative.[30] Thus, Figure 1c suggests that for submerged fibers cooperativity increases with the PEG concentration, which is the opposite of what was reported for the thermally induced helix-to-coil transition of polymers in solutions both for experimental[31] and theoretical[32] studies. This suggests that the changes in the width of the transition are primarily due to confinement.

It is worth noting that the changes in confinement are relatively small with the increasing PEG concentration but that the effects are relatively large. The diameter of a DNA molecule is 20 $Å^{-1}$. As shown in Table 1, the immersed fibers have only a few extra angstroms between the outer parts of neighboring molecules, but these result in a change of T_m by 10° and a drop in the width by ≈40% over the concentration range in Figure 1b,c.

Neutron Diffraction. Overall, the data are an improvement on the pilot study of DNA fibers submerged in PEG solutions.[11] The use of PEG solutions allowed the fibers to swell without losing their orientation. The neutron experiment was able to follow the evolution of the Bragg peak with temperature. The PBD model was able to describe the data, and the description was particularly good for the WOMBAT data. Fiber collapse appears to be less of a problem than for humidified fibers (cf. ref 11 and refs 6, 16); thus, the entire melting transition could be followed.

The previous study showed that the transition is, to an extent, reversible.[11] In this sense, it is similar to a critical phase transition. The diffuse scattering in Figure 5 increases rapidly at the melting temperature. The PEG6k-17% and PEG6k-20% samples show departures from a monotonic increase in the diffuse scattering intensity close to the melting temperature. These measurements suffered from relatively large temperature fluctuations around the melting temperature, and it is likely that the recorded intensity variations are a result of the time average of the concomitantly fluctuating diffuse signal. The measurements with better temperature stability at the melting transition did not show these anomalous intensity variations.

These variations do not appear to be present in the integrated intensities of the Bragg peaks of the affected samples. A Bragg peak is due to coherent scattering from a long-ranged, time-averaged order, whereas the diffuse scattering

DOI: 10.1021/acs.jpcb.7b11608
J. Phys. Chem. B XXXX, XXX, XXX−XXX

is more incoherent in nature. It may be that the diffuse scattering is dominated by the DNA dynamics, particularly of open base pairs, and its temperature dependence is driven by changes in the spectral weight. This hypothesis is consistent with the observation that D19, with the larger energy integration, shows a larger increase in the diffuse scattering.

The PBD model uses one set of parameters for DNA and is able to satisfactorily reproduce all of the data despite the change in confinement brought about by the osmotic pressure. This shows that the model is, within reasonable limits, insensitive to confinement of the DNA and establishes that the analysis shown in previous studies[6,7,16] is sound.

It is noteworthy that most of the parameters in Table 2 are the same as those for the humidified fibers[6,16] and for genomic DNA in solution.[24] The only differences lie in the values of D_{AT} and D_{GC}. Regarding the model, the unique effect of the submersion of the fibers on the melting transition seems to be in adjusting the apparent dissociation energy of the base pairs.

The success of the experimental configuration and the osmotic pressure method to characterize the spatial correlations throughout the DNA melting transition provides possibilities for investigating the dependence of the transition on a number of parameters. The sodium salt solution can be easily changed, providing opportunities to investigate the dependence of the transition on the cation type and concentration (e.g., refs 27 and 33). The melting of different conformations of DNA can be tested by replacing the PEG solution with an ethanol solution.[34] It is also possible to investigate the dependence on GC concentration,[27] although the sample preparation would require access to relatively large quantities of pure, genomic DNA with significantly different GC fractions. For reference, the GC concentrations for the two common commercially available DNA are 41.2% for the salmon testes used in the current study and 41.9% for DNA from calf thymus. These opportunities will be explored in future work.

CONCLUSIONS

Calorimetry data have shown that PEG affects the melting temperature and width of the melting transition of submerged DNA fibers independent of its molecular weight in the range studied. These effects seemed to be related mainly to the osmotic pressure applied by PEG varying the intermolecular distance. The PBD model was able to predict the melting curves of the submerged DNA by scaling the interaction between nucleotides by the melting temperature. A moderate variation of the confinement does not seem to be an issue for the application of the model. The results validate the use of the PBD model to describe complex DNA denaturation curves and include structural information that is lacking for a complete understanding of the transition.

AUTHOR INFORMATION

Corresponding Author

*E-mail: wildes@ill.fr. Phone: +33 476 207 037.

ORCID

Adrián González: 0000-0002-0965-0822

Notes

The authors declare no competing financial interest.

ACKNOWLEDGMENTS

We thank ANSTO and ILL for the beam time along with their staff. Special thanks to John Archer and Sebastien Vial for setting up the sample environment at D19. Special thanks also to Hervé Guillou for assistance when using the Nano-Calorimeter. A.G. thanks the PhD programme of the ILL for providing financial support for his thesis. N.T. acknowledges support by the project "Advanced Materials and Device" (MIS 5002409, NSRF 2014-2020) co-financed by Greece and the European Regional Development Fund.

REFERENCES

(1) Cuesta-López, S.; Angelov, D.; Peyrard, M. Adding a New Dimension to DNA Melting Curves. *EPL* **2009**, *87*, No. 48009.

(2) Tateishi-Karimta, H.; Sugimoto, N. Control of Stability and Structure of Nucleic Acids Using Cosolutes. *Methods* **2014**, *67*, 151−158.

(3) Wartell, R. M.; Benight, A. S. Thermal Denaturation of DNA Molecules: a Comparison of Theory with Experiment. *Phys. Rep.* **1985**, *126*, 67−107.

(4) Wittwer, C. T. High-Resolution DNA Melting Analysis: Advancements and Limitations. *Hum. Mutat.* **2009**, *30*, 857−859.

(5) Garibyan, L.; Avashia, N. Research Techniques Made Simple: Polymerase Chain Reaction (PCR). *J. Invest. Dermatol.* **2013**, *133*, No. e6.

(6) Wildes, A.; Theodorakopoulos, N.; Valle-Orero, J.; Cuesta-López, S.; Garden, J.-L.; Peyrard, M. Structural Correlations and Melting of B-DNA Fibers. *Phys. Rev. E* **2011**, *83*, No. 061923.

(7) Valle-Orero, J.; Wildes, A. R.; Theodorakopoulos, N.; Cuesta-López, S.; Garden, J.-L.; Danilkin, S.; Peyrard, M. Thermal Denaturation of A-DNA. *New J. Phys.* **2014**, *16*, No. 113017.

(8) Peyrard, M.; Bishop, A. R. Statistical Mechanics of a Nonlinear Model for DNA Denaturation. *Phys. Rev. Lett.* **1989**, *62*, 2755−2758.

(9) Yasar, S.; Podgornik, R.; Valle-Orero, J.; Johnson, M. R.; Parsegian, V. A. Continuity of States Between the Cholesteric-Line Hexatic Transition and the Condensation Transition in DNA Solutions. *Sci. Rep.* **2014**, *4*, No. 6877.

(10) Podgornik, R.; Stray, H. H.; Gawrisch, K.; Rau, D. C.; Rupprecht, A.; Parsegian, V. A. Bond Orientational Order, Molecular Motion, and Free Energy of High-Density DNA Mesophases. *Proc. Natl. Acad. Sci. U.S.A.* **1996**, *93*, 4261−4266.

(11) Wildes, A.; Khadeeva, L.; Trewby, W.; Valle-Orero, J.; Studer, A.; Garden, J.-L.; Peyrard, M. Melting of Highly Oriented Fiber DNA Subjected to Osmotic Pressure. *J. Phys. Chem. B* **2015**, *119*, 4441−4449.

(12) Rupprecht, A. Preparation of Oriented DNA by Wet Spinning. *Acta Chem. Scand.* **1966**, *20*, 494−504.

(13) Valle-Orero, J.; Garden, J.-L.; Richard, J.; Wildes, A.; Peyrard, M. Glassy Behaviour of Denatured DNA Films Studied by Differential Scanning Calorimetry. *J. Phys. Chem. B* **2012**, *116*, 4394−4402.

(14) Valle-Orero, J.; Wildes, A.; Garden, J.-L.; Peyrard, M. Purification of A-Form DNA Fiber Samples by the Removal of B-Form DNA Residues. *J. Phys. Chem. B* **2013**, *117*, 1849−1856.

(15) Rau, D. C.; Lee, B.; Parsegian, V. A. Measurement of the Repulsive Force between Polyelectrolyte Molecules in Ionic Solution: Hydration Forces between Parallel DNA Double Helices. *Proc. Natl. Acad. Sci. U.S.A.* **1984**, *81*, 2621−2625.

(16) Wildes, A.; Theodorakopoulos, N.; Valle-Orero, J.; Cuesta-López, S.; Garden, J.-L.; Peyrard, M. Thermal Denaturation of DNA Studied with Neutron Scattering. *Phys. Rev. Lett.* **2011**, *106*, No. 048101.

(17) Gonzalez, A.; Cristiglio, V.; Cuesta-López, S.; Demé, B.; Forsyth, T.; Garden, J.-L.; Johnson, M. R.; Marty-Roda, M.; Mossou, E.; Peyrard, M.; et al. DataCite Search. https://doi.org/10.5291/ill-data.9-13-625 (accessed Jan 11, 2018).

(18) Spink, C. H.; Chaires, J. B. Effects of Hydration, Ion Release, and Excluded Volume on the Melting of Triplex and Duplex DNA. *Biochemistry* **1999**, *38*, 496−508.

(19) Valle-Orero, J.; Wildes, A.; Garden, J.-L.; Peyrard, M. Purification of A-form DNA Fiber Samples by the Removal of B-Form DNA Residues. *J. Phys. Chem. B* **2013**, *117*, 1849−1856.

DOI: 10.1021/acs.jpcb.7b11608
J. Phys. Chem. B XXXX, XXX, XXX−XXX

(20) Langridge, R.; Wilson, H. R.; Hooper, C. W.; Wilkins, M. H. F.; Hamilton, L. D. The Molecular Configuration of Deoxyribonucleic Acid I. X-ray Diffraction Study of a Crystalline Form of the Lithium Salt. *J. Mol. Biol.* **1960**, *2*, 19−37.
(21) van Eijck, L.; Merzel, F.; Rols, S.; Ollivier, J.; Forsyth, V. T.; Johnson, M. R. Direct Determination of the Base-Pair Force Constant of DNA from Acoustic Phonon Dispersion of the Double Helix. *Phys. Rev. Lett.* **2011**, *107*, No. 088102.
(22) Dauxois, T.; Peyrard, M.; Bishop, A. R. Entropy-Diven DNA Denaturation. *Phys. Rev. E* **1993**, *47*, No. R44(R).
(23) Quinn, N. L.; Levenkova, N.; Chow, W.; Bouffard, P.; Boroevich, K. A.; Knight, J. R.; Jarvie, T. P.; Lubieniecki, K. P.; Desany, B. A.; Koop, B. F.; et al. Assesing the Feasibility of GS FLX Pyrosequencing for Sequencing the Atlantic Salmon Genome. *BMC Genomics* **2008**, *9*, No. 404.
(24) Theodorakopoulos, N. Melting of Genomic DNA: Predictive Modeling by Nonlinear Lattice Dynamics. *Phys. Rev. E* **2010**, *82*, No. 021905.
(25) Krisch, M.; Mermet, A.; Grimm, H.; Forsyth, V. T.; Rupprecht, A. Phonon Dispersion of Oriented DNA by Inelastic X-ray Scattering. *Phys. Rev. E* **2006**, *73*, No. 061909.
(26) Lavery, R.; Moakher, M.; Maddocks, J. H.; Petkeviciute, D.; Zakrewska, K. Conformational Analysis of Nucleic Acid Revisited: Curves+. *Nucleic Acids Res.* **2009**, *37*, 5917−5929.
(27) Grasso, D.; Fasone, S.; La Rosa, C.; Salyanov, V. A Calorimetric Study of the Different Thermal Behaviour of the DNA in the Isotropic and Liquid-Crystalline States. *Liq. Cryst.* **1991**, *9*, 299−305.
(28) Cherstvy, A. G.; Kornyshev, A. A. DNA Melting in Aggregates: Impeded or Facilitated. *J. Phys. Chem. B* **2005**, *109*, 13024−13029.
(29) Woolley, P.; Wills, P. R. Excluded-Volume Effect of Inert Macromolecules on the Melting of Nucleic Acids. *Biophys. Chem.* **1985**, *22*, 89−94.
(30) Spink, C. H. The Deconvolution of Differential Scanning Calorimetry Unfolding Transitions. *Methods* **2015**, *76*, 78−86.
(31) Koutsioubas, A.; Lairez, D.; Combet, S.; Fadda, G. C.; Longeville, S.; Zalczer, G. Crowding Effect on Helix-Coil Transition: Beyond Entropic Stabilization. *J. Chem. Phys.* **2012**, *136*, No. 215101.
(32) Badasyan, A.; Tonoyan, S.; Giacometti, A.; Podgornik, R.; Parsegian, V. A.; Mamasakhlisov, Y.; Morozov, V. Osmotic Pressure Induced Coupling between Cooperativity and Stability of a Helix-coil Transition. *Phys. Rev. Lett.* **2012**, *109*, No. 068101.
(33) Cherstvy, A. G.; Kornyshev, A. A.; Leikin, S. Temperature-Dependent DNA Condensation Triggered by Rearrangement of Adsorbed Cations. *J. Phys. Chem. B* **2002**, *106*, 13362−13369.
(34) Rupprecht, A.; Piškur, J.; Schultz, J.; Nordenskiöld, L.; Song, Z.; Lahajnar, G. Mechanochemical Study of Conformational Transitions and Melting of Li-, Na-, K-, and CsDNA Fibers in Ethanol-Water Solutions. *Biopolymers* **1994**, *34*, 897−920.

DOI: 10.1021/acs.jpcb.7b11608
J. Phys. Chem. B XXXX, XXX, XXX−XXX